PNAS RESEARCH ARTICLE | CELL BIOLOGY OPEN ACCESS

Drug repurposing screen identifies an HRI activating compound that promotes adaptive mitochondrial remodeling in MFN2-deficient cells

Prerona Bora[a,1], Mashiat Zaman[b,1], Samantha Oviedo[a,c], Sergei Kutseikin[a], Nicole Madrazo[a], Prakhyat Mathur[a,c], Meera Pannikkat[a], Sophia Krasny[a], Rama Aldakhlallah[a], Alan Chu[d], Kristen A. Johnson[d], Danielle A. Grotjahn[c], Timothy E. Shutt[e,f,2], and R. Luke Wiseman[a,2]

Affiliations are included on p. 11.

Edited by Peter Walter, Altos Labs, San Francisco, CA; received July 10, 2025; accepted October 11, 2025

Pathogenic variants in the mitochondrial outer membrane GTPase MFN2 cause the peripheral neuropathy Charcot–Marie–Tooth type 2A (CMT2A). These mutations can disrupt MFN2-dependent regulation of diverse aspects of mitochondrial biology including organelle morphology, motility, mitochondrial-endoplasmic reticulum (ER) contacts (MERCs), and respiratory chain activity. However, no therapies currently exist to mitigate the mitochondrial dysfunction linked to genetic deficiencies in MFN2. Herein, we performed a drug repurposing screen to identify compounds that selectively activate the integrated stress response (ISR)—the predominant stress-responsive signaling pathway responsible for regulating mitochondrial morphology and function. This screen identified the compounds parogrelil and MBX-2982 as potent and selective activators of the ISR through the OMA1-DELE1-HRI signaling axis. We show that treatment with these compounds promotes adaptive, ISR-dependent remodeling of mitochondrial morphology and protects mitochondria against genetic and chemical insults. Moreover, we show that pharmacologic ISR activation afforded by parogrelil restores mitochondrial tubular morphology, promotes mitochondrial motility, rescues MERCs, and enhances mitochondrial respiration in *MFN2*-deficient cells. These results demonstrate the potential for pharmacologic ISR activation through the OMA1-DELE1-HRI signaling pathway as a potential strategy to mitigate mitochondrial dysfunction in CMT2A and other pathologies associated with MFN2 deficiency.

integrated stress response | drug repurposing | mitochondrial dysfunction

Significance

Here, we performed a drug repurposing screen that identified compounds that selectively activate the integrated stress response (ISR) through the OMA1-DELE1-HRI signaling axis. Using these compounds, and another ISR activating compound that targets the alternative ISR kinase GCN2, we show that pharmacologic ISR activation mitigates multiple pathologies linked to reduced activity of the mitochondrial GTPase MFN2. These results suggest pharmacologic ISR activation as a strategy to ameliorate pathologies in disorders linked to MFN2 deficiency, such as Charcot–Marie–Tooth type 2A.

While originally defined for its role in promoting mitochondrial fusion, the outer mitochondrial membrane (OMM) GTPase MFN2 is now recognized to have additional functions, including the maintenance of mitochondrial-endoplasmic reticulum (ER) contacts (MERCs) and mediating mitochondrial motility (1–4). These primary functions of MFN2 can lead to secondary roles for this protein involved in regulating other aspects of mitochondrial biology including respiration (5–10). Consistent with the importance of MFN2 for mitochondrial function, >180 pathogenic variants localized throughout the MFN2 protein are causatively associated with the neurological disease Charcot–Marie–Tooth type 2A (CMT2A), a genetic peripheral neuropathy involving axonal degeneration and dysfunction (8, 11). Most pathogenic MFN2 variants are autosomal dominant heterozygous missense variants. However, there are reports of deletion variants (7, 12) and examples of autosomal recessive inheritance [both homozygous (5, 9, 13) and compound heterozygous (13–15)]. Further complicating the issue is the fact that some pathogenic MFN2 variants cause other disease phenotypes that are separate and/or in addition to peripheral neuropathy [e.g., ataxia (9), areflexia (5), distal myopathy (10), hypotonia (5), optic atrophy (9), sensorineural hearing loss (9), and multiple symmetric lipomatosis (16)]. The mechanistic basis by which MFN2 dysfunction leads to CMT2A and related pathologies is not fully understood (8). Consistent with a loss-of-function disease mechanism, reduced fusion of the mitochondrial network (11, 17, 18), decreased ER–mitochondrial contacts (1, 19), and impaired mitochondrial motility (11, 20) have all been implicated. However, only a handful of MFN2 variants have been studied functionally. Further, the fact that MFN2 has multiple distinct functions precludes a simplistic view on disease mechanism.

With CMT2A accounting for 30-40% of all axonal cases of CMT2 (21–23), significant effort has been directed at developing therapeutic strategies to mitigate these pathologic mitochondrial dysfunctions associated with impaired MFN2 activity. These include strategies to enhance activity of the alternative OMM GTPase MFN1 (17, 24, 25), genetically replace pathogenic MFN2 alleles (26), and promote MFN2 activity (27–31). However, while

Preprint server: This article was posted as a preprint to bioRXIV (doi: https://doi.org/10.1101/2025.06.23.660251).

Author contributions: P.B., M.Z., K.A.J., D.A.G., T.E.S., and R.L.W. designed research; P.B., M.Z., S.O., S. Kutseikin, P.M., M.P., S. Krasny, R.A., and A.C. performed research; P.B., M.Z., S.O., S. Kutseikin, N.M., P.M., M.P., S. Krasny, R.A., A.C., K.A.J., D.A.G., T.E.S., and R.L.W. analyzed data; and P.B., M.Z., T.E.S., and R.L.W. wrote the paper.

The authors declare no competing interest.

This article is a PNAS Direct Submission.

[1]P.B. and M.Z. contributed equally to this work.

[2]To whom correspondence may be addressed. Email: timothy.shutt@ucalgary.ca or wiseman@scripps.edu.

This article contains supporting information online at https://www.pnas.org/lookup/suppl/doi:10.1073/pnas.2517552122/-/DCSupplemental.

Published November 25, 2025.

progress has been made, no therapeutic approaches are currently available to ameliorate the pathologic mitochondrial dysfunction implicated in the pathogenesis of MFN2-associated CMT2A.

Another potential strategy to mitigate mitochondrial dysfunction associated with MFN2 deficiency is to pharmacologically enhance the activity of adaptive stress-responsive signaling pathways that regulate mitochondrial morphology and function. The integrated stress response (ISR) has emerged as the predominant signaling pathway responsible for adapting mitochondrial biology in mammalian cells. The ISR comprises four stress-activated kinase—GCN2, HRI, PERK, and PKR—that are activated in response to diverse types of pathologic insults including amino acid deprivation, mitochondrial stress, ER stress, and viral infection, respectively (32, 33). Upon activation, these kinases selectively phosphorylate the α subunit of eukaryotic initiation factor 2 (eIF2α), resulting in both the attenuation of new protein synthesis and the activation of stress-responsive transcription factors such as ATF4 (32, 33). ISR-dependent transcriptional and translational signaling regulates many aspects of mitochondrial biology such as proteostasis, morphology, lipid synthesis, and respiratory chain activity (34–41). Notably, ISR-dependent translational attenuation promotes mitochondrial elongation during ER stress downstream of PERK through a mechanism involving inhibition of the profission mitochondrial GTPase DRP1 (35, 37). This finding suggests that pharmacologically enhancing ISR signaling offers a potential opportunity to mitigate pathologic mitochondrial fragmentation and subsequent organelle dysfunctions linked to MFN2 deficiency.

Consistent with this idea, pharmacologic activation of ISR kinases has proven beneficial for mitigating mitochondrial fragmentation and dysfunction in cellular models of diverse diseases. For example, treatment with the glutamyl-prolyl tRNA synthetase inhibitor halofuginone—a compound that activates the ISR kinase GCN2 (42)—promotes adaptive mitochondrial elongation and restores mitochondrial morphology and respiratory chain activity in cells deficient in the ISR kinase PERK (34, 36). Similarly, pharmacologic activation of PERK or GCN2 mitigates mitochondrial fragmentation induced by the calcium ionophore ionomycin (34). However, despite this promise, currently available strategies to activate the ISR are limited in their translational potential for diseases like CMT2A by factors including poor selectivity for the ISR, low potency, dosing limitations, and off-target activities that directly impact mitochondrial biology (36). For example, the compound BtdCPU was previously shown to activate the ISR kinase HRI by inducing mitochondrial uncoupling, precluding its use for correcting mitochondrial dysfunction in MFN2-deficient cells (36). Further, other ISR activators including halofuginone or ATP competitive inhibitors of ISR kinases can induce ISR-independent translational inhibition or inhibit ISR kinase activity, respectively, at certain concentrations (43–45). Thus, new compounds are required to access adaptive ISR-dependent mitochondrial remodeling to further probe the potential for pharmacologic ISR activation to mitigate mitochondrial dysfunction associated with MFN2 deficiency.

Here, we employed a drug-repurposing screen to identify highly selective ISR activators with improved potential for mitigating mitochondrial dysfunction induced by reduced MFN2 activity. We screened the ReFRAME drug repurposing library comprising compounds previously shown to have promising safety profiles in human trials to identify compounds that selectively activate the ISR (46). This approach identified two compounds, parogrelil and MBX-2982, which activate the ISR with transcriptome-wide selectivity. Intriguingly, these compounds both activate the ISR through the OMA1-DELE1-HRI signaling axis; however, they do not induce the mitochondrial dysfunction commonly associated with this activation mechanism (e.g., uncoupling, organelle fragmentation). Instead, we show that parogrelil and MBX-2982 promote ISR-dependent mitochondrial elongation in mammalian cell culture models and reduce mitochondrial fragmentation induced by chemical or genetic insults. Finally, we show that pharmacologic ISR activation using parogrelil or the GCN2 activator halofuginone mitigates diverse aspects of mitochondrial dysfunction in MFN2-deficient cells including morphology, motility, ER–mitochondrial contacts, and respiration. Collectively, these results demonstrate the potential for pharmacologic ISR activators to promote adaptive mitochondrial remodeling and mitigate mitochondrial dysfunction in MFN2-deficient cells, establishing pharmacologic ISR activation as a potential strategy to ameliorate mitochondrial dysfunction in CMT2A and other diseases linked to reduced MFN2 activity.

Results

Screening of the ReFRAME Library to Identify ISR Activating Compounds. We screened the 15,480 molecule ReFRAME drug repurposing library (46) to identify compounds that activate the ATF4-FLuc ISR reporter stably expressed in HEK293T cells (Fig. 1*A*) (47). The ER stressor thapsigargin (Tg) was used as a positive control for this primary screen to demonstrate robustness of the screening assay (robust Z' factor = 0.5; S/N 2.53). Our primary screen identified 153 compounds that showed ATF4-FLuc activation that was >90% that observed for Tg (Dataset S1). These compounds were then subjected to dose–response screening to define their EC_{50} for ATF4-FLuc activation (robust Z' for dose–response screen = 0.47). This analysis identified 112 "hit" compounds with a measurable EC_{50} less than 10 μM (Dataset S1). These hits included numerous compounds that activate the ISR through known mechanisms including proteasome inhibition (e.g., bortezomib) or mitochondrial stress (e.g., antimycin A), validating the efficacy of our assay. To prioritize compounds for further study, we focused on compounds with: 1) high potency for ATF4-FLuc activation, 2) low toxicity in HEK293T cells, as measured in previous screens performed at TSRI-CALIBR, 3) compound structures suitable for continued development, and 4) effective safety profiles. From this prioritization, we selected five compounds for further study—ciclesonide, capadenoson, velsecorat, MBX-2982, and parogrelil (Fig. 1*B* and *SI Appendix*, Fig. S1*A*). We repurchased these compounds and retested their ability to activate the ATF4-FLuc reporter. Repurchased ciclesonide, capadenoson, and velsecorat did not potently activate the ATF4-FLuc reporter (*SI Appendix*, Fig. S1*B*). Further, these repurchased compounds did not induce expression of the ISR target genes *CHAC1* and *ASNS* in HEK293T cells (*SI Appendix*, Fig. S1*C*). Thus, we excluded these compounds from further study. In contrast, MBX-2982 (MBX) and parogrelil (PGL) both activated the ATF4-FLuc reporter with similar potency to that observed in our original screen (Fig. 1*C*) and did not show cytotoxicity in HEK293T cells (*SI Appendix*, Fig. S1*D*). Cotreatment with the ISR inhibitor ISRIB—a compound that desensitizes cells to ISR-dependent phosphorylation of eIF2α (48–51)—blocked ATF4-FLuc activation induced by MBX and PGL (Fig. 1*D*). This finding demonstrated that these compounds activate the ATF4-FLuc ISR reporter through an ISR-dependent mechanism. We then confirmed that MBX and PGL induced expression of the ISR target genes *CHAC1* and *ASNS* and showed dose-dependent increases in the expression of the ISR-regulated transcription factor ATF4 in HEK293T cells (Fig. 1 *E*–*G*). We also saw an increase in phosphorylated eIF2α in cells treated with MBX

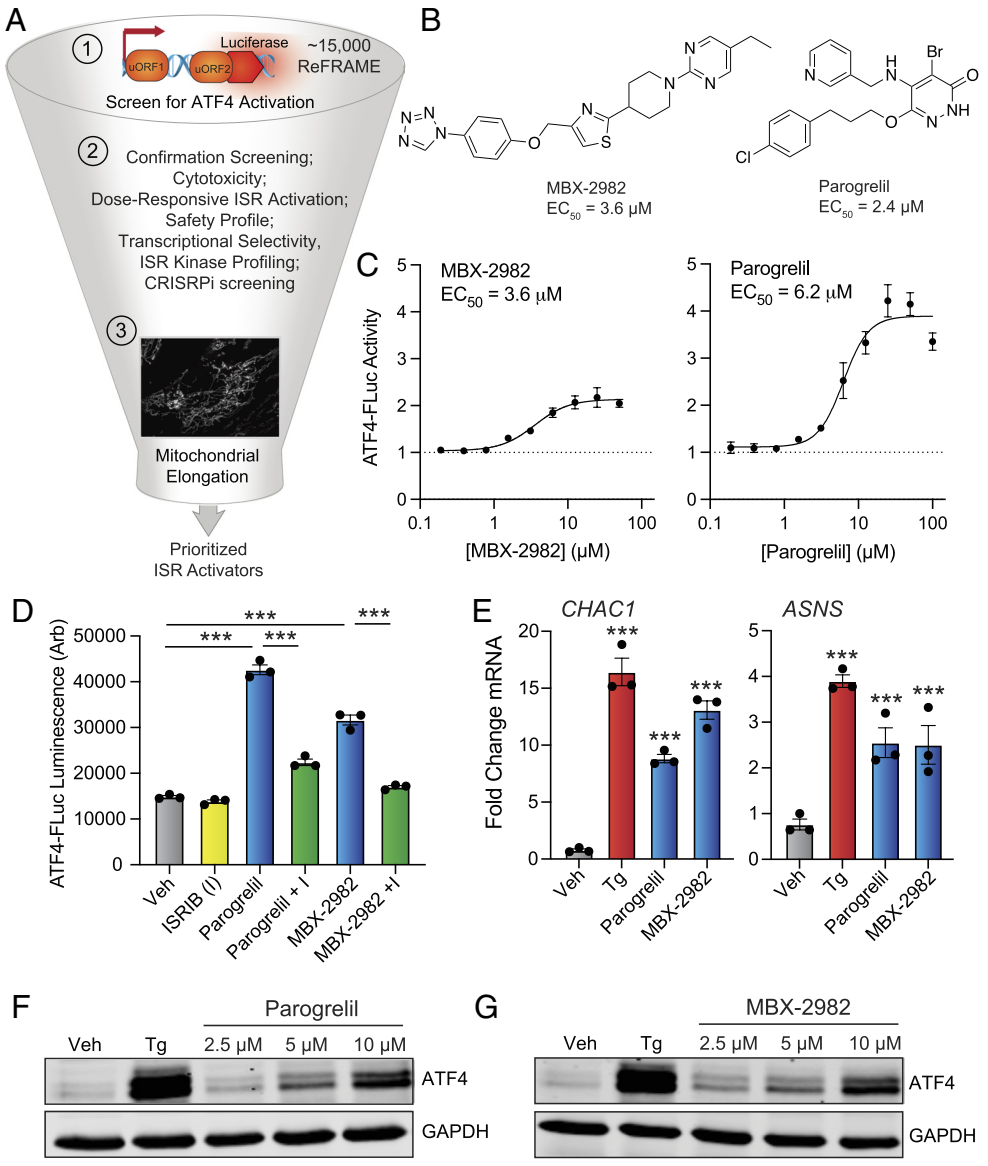

Fig. 1. High-throughput screening of the ReFRAME library identifies ISR activating compounds. (*A*) Schematic of the HTS pipeline used to screen the ReFRAME library. (*B*) Structures of the prioritized ISR activating compounds MBX-2982 and parogrelil. The EC_{50} for activation of the ATF4-FLuc ISR reporter determined from our primary screen is shown. (*C*) ATF4-FLuc activation in HEK293T cells treated for 8 h with the indicated concentration of repurchased MBX-2982 (*Left*) or parogrelil (*Right*). The EC_{50} for experiments with the repurchased compounds are shown. (*D*) ATF4-FLuc activation in HEK293T cells treated for 8 h with parogrelil (10 μM), MBX-2982 (10 μM), and/or ISRIB (I; 200 nM). Error bars show SEM for n = 3 replicates. (*E*) Expression, measured by RT-qPCR, of the ISR target genes *CHAC1* or *ASNS* in HEK293T cells treated for 6 h with thapsigargin (Tg; 500 nM), MBX-2982 (10 μM), or parogrelil (10 μM). Error bars show SEM for n = 3 replicates. (*F* and *G*) Immunoblots of lysates prepared from HEK293T cell treated for 6 h with thapsigargin (Tg; 500 nM) or the indicated dose of parogrelil (*F*) or MBX-2982 (*G*). ***$P < 0.005$ for one-way ANOVA. Panel *E* statistics are shown relative to vehicle-treated cells.

or PGL, further highlighting the activation of the ISR afforded by these compounds (*SI Appendix*, Fig. S1*E*). This work identified MBX and PGL as nontoxic ISR activating compounds that we prioritized for further study.

MBX-2982 and Parogrelil Are Highly Selective Activators of ISR Signaling. We next defined the selectivity of ISR activation afforded by MBX and PGL. We performed RNAseq in HEK293T cells treated for 6 h with these compounds (Dataset S2). Intriguingly, the genes most significantly induced by these compounds were known transcriptional targets of the ISR (e.g., *CHAC, DDIT4, STC2*; Fig. 2 *A* and *B*). Consistent with this observation, treatment with MBX and PGL increased expression of a geneset comprising target genes regulated by the ISR, albeit to a lesser extent than that observed for the potent ISR activators Tg or oligomycin (Fig. 2 *C* and *D*, *SI Appendix*, Fig. S2*A*, and Dataset S3) (52). However, we did not see significant increases in genesets comprising target genes of other stress-responsive signaling pathways such as the ATF6 and IRE1/XBP1s arms of the unfolded protein response (UPR), heat shock response (HSR), oxidative stress response (OSR), or hypoxic stress response (52). ISR selectivity was also observed in HEK293T cells treated with the mitochondrial toxin oligomycin (53), but not in Tg-treated cells (*SI Appendix*, Fig. S2 *A*–*C*). Other ISR activators including halofuginone and BtdCPU also show similar selectivity for the ISR in cell culture models (54). We further confirmed selective ISR activation afforded by MBX and PGL with RT-qPCR, monitoring expression of UPR (e.g.,

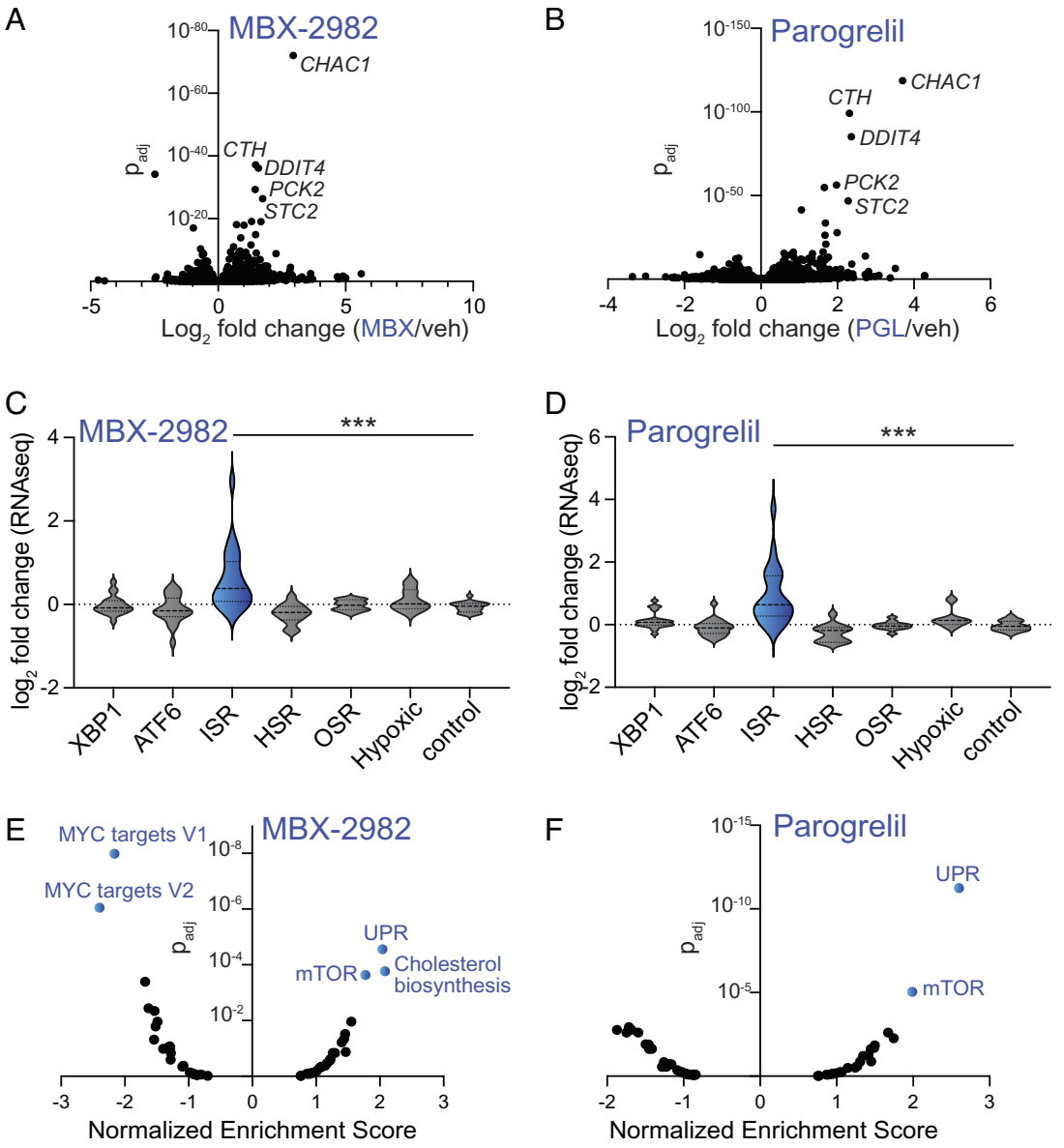

Fig. 2. MBX-2982 and parogrelil selectively activate the ISR. (*A* and *B*) Log_2 fold change vs. adjusted *P*-value (p_{adj}) of gene expression, measured by RNAseq, in HEK293T cells treated for 6 h with MBX-2982 (10 μM, *A*) or parogrelil (10 μM, *B*). RNAseq data are shown in Dataset S2. (*C* and *D*) Expression, measured by RNAseq of genesets comprising target genes of the XBP1s or ATF6 arms of the UPR, ISR, HSR, OSR, or hypoxic stress response in HEK293T cells treated for 6 h with MBX-2982 (10 μM) or parogrelil (10 μM). A geneset comprising control genes is shown as a control. Genesets are described in Dataset S3. ***$P < 0.005$ for one-way ANOVA. (*E* and *F*) Normalized enrichment score vs. adjusted *P*-value (p_{adj}) for geneset activation, measured by GSEA, in HEK293T cells treated for 6 h with MBX-2982 (10 μM; *E*) or parogrelil (10 μM; *F*). Full GSEA is shown in Dataset S4.

BiP, *XBP1s*), HSR (e.g., *HSPA1A*), and OSR (e.g., *NQO1*) target genes (*SI Appendix*, Fig. S2*D*). These results indicate that MBX and PGL preferentially activate the ISR. Further supporting this idea, geneset enrichment analysis (GSEA) showed increased expression of UPR and mTOR genesets—two genesets that include many ISR target genes—in HEK293T cells treated with MBX or PGL (Fig. 2 *E* and *F*). Similar increases in these genesets were observed for other potent ISR activators including the ER stressor Tg and the mitochondrial toxin oligomycin (*SI Appendix*, Fig. S2 *E* and *F*) (53). However, MBX also induced expression of the cholesterol biosynthesis geneset and suppressed expression of MYC target genesets, suggesting that this compound may have additional activity. These results indicate that MBX and, to a greater extent, PGL show transcriptome-wide selectivity for the ISR, particularly among stress-responsive signaling pathways.

MBX and PGL Activate ISR Signaling through the OMA1-DELE1-HRI Signaling Axis. We next sought to define the mechanism by which PGL and MBX activate the ISR. Cotreatment of HEK293T cells with both PGL and MBX did not significantly increase expression of the ISR target gene *ASNS* above that observed in cells treated with each compound alone, suggesting that these compounds activate the ISR through similar mechanisms (*SI Appendix*, Fig. S3*A*). We next treated HEK293T cells stably expressing ATF4-mAPPLE CRISPRi depleted of individual ISR kinases with these compounds and monitored ISR activation by mAPPLE fluorescence (53). CRISPRi-depletion of *HRI*, but no other ISR kinases, blocked ISR activation induced by treatment with MBX or PGL (Fig. 3*A* and *SI Appendix*, Fig. S3*B*). Similarly, *HRI* depletion blocked expression of ISR target genes (e.g., *CHAC1*, *ASNS*) and increases of ATF4 protein in HEK293T cells

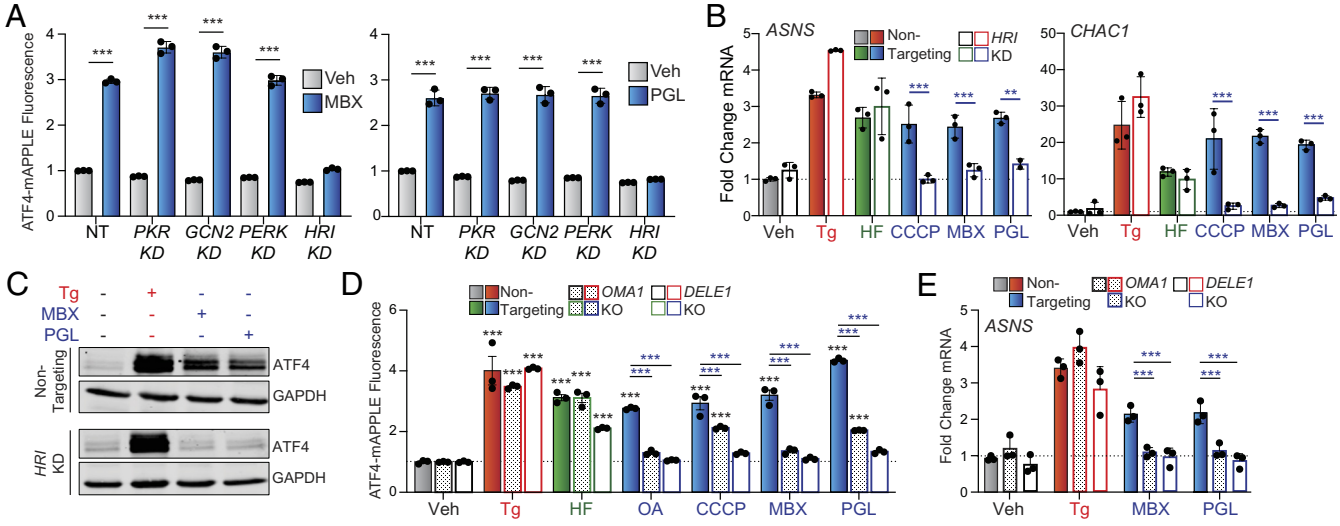

Fig. 3. MBX-2982 and parogrelil activate the ISR through the OMA1-DELE1-HRI signaling axis. (*A*) Activation of the ATF4-mAPPLE ISR reporter in HEK293T cells CRISPRi-depleted of the indicated ISR kinase treated for 16 h with MBX-2982 (MBX; 10 μM; *Left*) or parogrelil (PGL; 10 μM; *Right*). (*B*) Expression, measured by RT-qPCR, of the ISR target genes *ASNS* and *CHAC1* in nontargeting HEK293T cells or HEK293T cells CRISPRi-depleted *HRI* treated for 6 h with thapsigargin (Tg; 500 nM), halofuginone (100 nM), CCCP (10 μM), MBX-2982 (MBX; 10 μM), or parogrelil (PGL; 10 μM). (*C*) Immunoblot of lysates prepared from nontargeting HEK293T cells (*Top*) or HEK293T cells CRISPRi-depleted *HRI* (*Bottom*) treated for 6 h with thapsigargin (Tg; 500 nM), MBX-2982 (MBX; 10 μM), or parogrelil (PGL; 10 μM). (*D*) Activation of the ATF4-mAPPLE ISR reporter in HEK293T cells CRISPR-deleted of *OMA1* or *DELE1* treated for 16 h with thapsigargin (Tg; 500 nM), halofuginone (100 nM), oligomycin A (OA; 500 nM), CCCP (10 μM), MBX-2982 (MBX; 10 μM), or parogrelil (PGL; 10 μM). (*E*) Expression, measured by RT-qPCR, of the ISR target gene *ASNS* in nontargeting HEK293T cells or HEK293T cells CRISPR-deleted of *OMA1* or *DELE1* treated for 6 h with thapsigargin (Tg; 500 nM), MBX-2982 (MBX; 10 μM), or parogrelil (PGL; 10 μM). Error bars show SEM for n = 3 replicates. ***$P < 0.005$ for one-way ANOVA (panel *A*) or two-way ANOVA (panels *B*, *D*, and *E*). Black asterisks show comparison with vehicle-treated controls. Colored asterisks show comparison for a given treatment across genotypes.

treated with these two compounds (Fig. 3 *B* and *C*). These results indicate that both MBX and PGL activate the ISR kinase HRI.

HRI is activated by diverse mechanisms including reductions in intracellular heme and proteolytic processing of the mitochondrial-targeted HRI adaptor protein DELE1 by the mitochondrial inner membrane protease OMA1 (47, 53, 55, 56). Thus, we sought to determine the dependence of MBX- and PGL-dependent HRI activation on these two mechanisms. We initially monitored ATF4-FLuc activation in HEK293T cells cotreated with the heme analog hemin (to reverse potential effects of heme depletion) and MBX or PGL. Cotreatment with hemin did not impair the ability for these compounds to activate this ISR reporter (*SI Appendix*, Fig. S3*C*). This finding suggests that these compounds do not influence HRI activation through a mechanism involving reductions in intracellular heme. Next, we probed the impact of CRISPR deletion of *OMA1* or *DELE1* on ATF4-mAPPLE activation in HEK293T cells treated with MBX or PGL. *OMA1* deletion partially inhibited ATF4-mAPPLE activation induced by MBX or PGL, while *DELE1* deletion completely inhibited ATF4-mAPPLE activation afforded by these compounds (Fig. 3*D*). Similar results were observed for oligomycin and carbonyl cyanide 3-chlorophenylhydrazone (CCCP; Fig. 3*D*)—two compounds previously shown to activate OMA1-DELE1-HRI signaling (53, 56). In contrast, deletion of *OMA1* or *DELE1* did not significantly impact ATF4-mAPPLE activation afforded by treatment with the ER stressor thapsigargin (Tg) or the GCN2 activator halofuginone (HF), although we did observe a modest reduction in HF-dependent ATF4-mAPPLE fluorescence in *DELE1*-deleted cells. We further confirmed that *DELE1* or *OMA1* deletion impaired expression of ISR target genes (e.g., *ASNS*, *CHAC1*) and increases in ATF4 protein expression in HEK293T cells treated with MBX or PGL (Fig. 3*E* and *SI Appendix*, Fig. S3 *D*–*F*). Similar results were observed for other compounds that activate the OMA1-DELE1-HRI signaling pathway including BtdCPU and oligomycin, but not the PERK activator Tg or the GCN2 activator HF. These results indicate that MBX and PGL activate the ISR through the OMA1-DELE1-HRI signaling axis.

MBX-2982 and Parogrelil Rescue Mitochondrial Fragmentation Induced by Pharmacologic or Genetic Insults. Activation of OMA1-DELE1-HRI signaling can be induced by mitochondrial stressors such as the uncoupler CCCP or the ATP synthase inhibitor oligomycin, both of which also induce mitochondrial fragmentation (53, 56). Neither MBX nor PGL significantly impacted mitochondrial membrane potential in HEK293T cells, as measured by TMRE staining (*SI Appendix*, Fig. S4*A*). Further, treatment with these compounds did not promote mitochondrial fragmentation in MEF cells (Fig. 4 *A*–*C*). Instead, both MBX and PGL increased mitochondrial length and reduced organelle sphericity in these cells, indicating that pharmacologic HRI activation promotes mitochondrial elongation—an adaptive phenotype previously shown to be induced by activation of other ISR kinases (34, 35, 37, 54). Cotreatment with the ISR inhibitor ISRIB blocked mitochondrial elongation induced by these two compounds, indicating that this phenotype can be attributed to ISR activation (Fig. 4 *A*–*C*). Similar results were observed with the ER stressor thapsigargin—an activator of the ISR kinase PERK—as previously reported (35, 37, 54). We confirmed that treatment with MBX or PGL induced expression of ISR target genes (e.g., *Asns*, *Chop*, *Chac1*) in MEFs by RT-qPCR (*SI Appendix*, Fig. S4*B*). Further, we show that PGL and MBX induce mitochondrial elongation in cells lacking the ISR transcription factor ATF4, suggesting that mitochondrial elongation induced by these compounds is independent of ATF4 activity (*SI Appendix*, Fig. S4 *C* and *D*). This finding mirrors previous results showing that mitochondrial elongation induced by other ISR activators such as thapsigargin (Tg) or halofuginone (HF) proceeds through an ATF4-independent mechanism, instead being primarily mediated through ISR-dependent translation attenuation (35, 37, 54). These results show that MBX and PGL promote OMA1-DELE1-HRI signaling independent of mitochondrial uncoupling or mitochondrial fragmentation.

Our ability to promote ISR-dependent mitochondrial elongation using MBX or PGL suggests that treatment with these

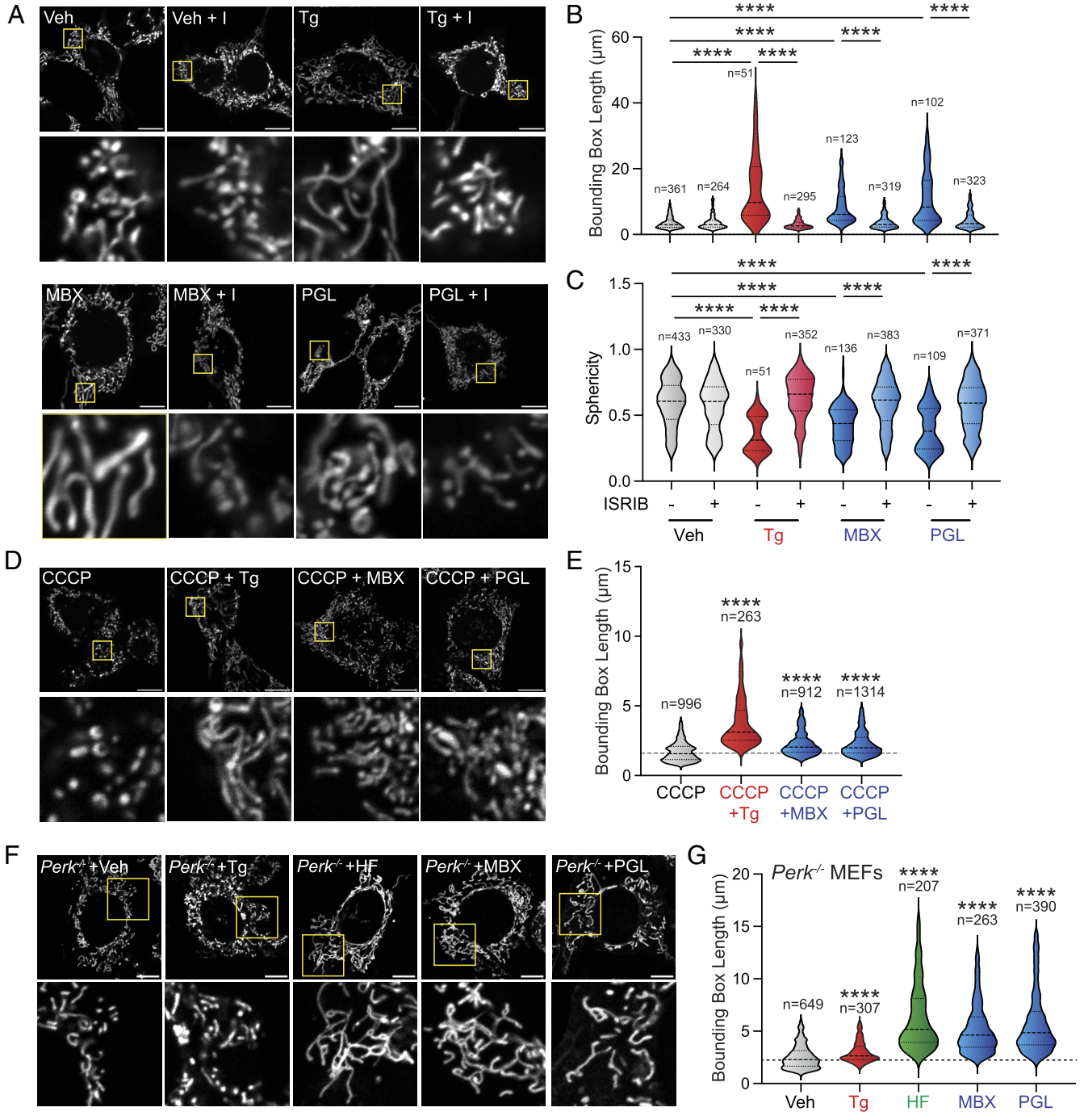

Fig. 4. MBX and PGL promote protective mitochondrial elongation. (*A*) Representative images of MEF cells stably expressing ^{mt}GFP (MEF^{mtGFP}) treated for 6 h with thapsigargin (Tg; 500 nM), MBX-2982 (MBX; 10 μM), or parogrelil (PGL; 10 μM) with or without ISRIB (200 nM). The *Inset* shows a threefold magnification of the region shown by the yellow box. (Scale bars 10 μm.) (*B* and *C*) Quantification of bounding box axis (*B*) and sphericity (*C*) from the entire dataset of images shown in (*A*). The number of mitochondrial measurements from >30 cells is shown. (*D*) Representative images of MEF cells stably expressing ^{mt}GFP (MEF^{mtGFP}) pretreated for 30 min with CCCP (10 μM) followed by 3 h treatment Tg (500 nM), MBX-2982 (MBX; 10 μM), or parogrelil (PGL; 10 μM). The *Inset* shows a threefold magnification of the region shown by the yellow box. (Scale bars 10 μm.) (*E*) Quantification of bounding box axis from the entire dataset of images shown in *D*. The number of mitochondrial measurements from >25 cells is shown. (*F*) Representative images of TMRE stained *Perk*$^{-/-}$ MEF cells treated for 6 h with veh, Tg (500 nM), MBX-2982 (MBX; 10 μM), or parogrelil (PGL; 10 μM). The *Inset* shows a threefold magnification of the region shown by the yellow box. (Scale bars 10 μm.) (*G*) Quantification of bounding box axis from the entire dataset of images shown in *F*. The number of mitochondrial measurements from >20 cells is shown. ****$P < 0.001$ for the Kruskal–Wallis test. In panels *E* and *G*, comparisons are shown relative to vehicle-treated cells.

compounds could mitigate pathologic mitochondrial fragmentation induced by chemical or genetic insults. To test this notion, we pretreated MEF cells with the mitochondrial uncoupler CCCP for 30 min to induce mitochondrial fragmentation then monitored mitochondrial morphology in these cells following 3 h treatment with MBX or PGL. The ER stressor and ISR activator thapsigargin (Tg) was used as a control. Treatment with either MBX or PGL reduced mitochondrial sphericity and increased mitochondrial length in CCCP-treated cells (Fig. 4 *D* and *E* and *SI Appendix*, Fig. S4*E*). Further, we showed that MBX or PGL rescued mitochondrial tubular morphology in MEF cells lacking the ISR kinase PERK (Fig. 4 *F* and *G* and *SI Appendix*, Fig. S4

F–K) (57)—a genetic perturbation previously shown to increase mitochondrial fragmentation (54). Collectively, these results indicate that MBX and PGL can both mitigate mitochondrial fragmentation induced by chemical or genetic insults.

Pharmacologic ISR Activation Promotes Adaptive Mitochondrial Remodeling in MFN2-Deficient Cells. MFN2 deficiency leads to pathologic mitochondrial dysfunctions implicated in CMT2A including organelle fragmentation, reduced motility, and decreased MERCs (8). We sought to define the potential for pharmacologic ISR activation with MBX or PGL to mitigate these phenotypes in *Mfn2* knockout MEFs (4) and U2OS cells CRISPR-deleted of *MFN2*. We also treated these cells with the GCN2 activator halofuginone (HF). Treatment with HF or PGL for 6 h restored mitochondrial morphology to near wild-type levels in MFN2-deficient MEF and U2OS cells (Fig. 5 *A–C* and *SI Appendix*, Fig. S5 *A–C*). Cotreatment with ISRIB blocked compound-dependent mitochondrial elongation in MFN2-deficient cells, confirming that this effect can be attributed to ISR activity. In contrast, MBX only modestly increased mitochondrial length in *Mfn2*-deficient MEFs and increased mitochondrial fragmentation in *MFN2*-deficient U2OS cells (Fig. 5 *A–C*). This latter effect appears to be dependent on MFN2 deficiency, as treatment with MBX induced mitochondrial elongation in *MFN2*-deficient U2OS cells reexpressing $MFN2^{WT}$ (*SI Appendix*, Fig. S5*C*). This observation suggests a synthetic interaction between MBX and MFN2 deficiency that precludes the ability for this compound to promote adaptive mitochondrial remodeling in cells lacking MFN2. Thus, we excluded MBX from further studies in MFN2-deficient cells. Regardless, our results show that pharmacologic ISR activation with the GCN2 activator HF or the HRI activator PGL restores mitochondrial morphology in cells deleted of MFN2.

MFN2 deficiency increases perinuclear clustering of mitochondria (Fig. 5 *D–F* and *SI Appendix*, Fig. S5 *D–F*). This observation is attributed to disruptions in mitochondrial trafficking (i.e., motility) in cells lacking MFN2 (4). Treatment with the HRI activator PGL increased mitochondrial distribution in both wild-type and MFN2-deficient U2OS and MEF cells (Fig. 5 *D–F* and *SI Appendix*, Fig. S5 *D–F*). This increase was blocked by cotreatment with ISRIB. However, treatment with the GCN2 activator HF only modestly increased mitochondrial distribution in MFN2-deficient U2OS cells, but did not influence mitochondrial distribution in wild-type U2OS, wild-type MEFs, or *Mfn2*-deficient MEFs. The increased mitochondrial distribution observed in PGL-treated wild-type and MFN2-deficient cells likely reflects increased mitochondrial motility. To test this idea, we used live cell time-lapse imaging to quantify the distance mitochondria travel in *MFN2*-deficient U2OS treated with ISR activators. This work showed that PGL treatment increased the distance mitochondria travel in both wild-type and *MFN2*-deficient U2OS through an ISRIB-sensitive mechanism (Fig. 5 *G* and *H* and Movie S1). Similar results were observed in wild-type and *Mfn2* KO MEFs (*SI Appendix*, Fig. S5 *G* and *H*). HF treatment also modestly increased the distance mitochondrial traveled in wild-type and MFN2-deficient U2OS and MEF cells, albeit to a lesser extent than that observed for PGL. Together, these results show that pharmacologic ISR activation, especially PGL-dependent HRI activation, restores organellar distribution and enhances mitochondrial motility in MFN2-deficient cells.

MFN2 facilitates formation and stability of MERCs (1). While there is debate over the specific role of MFN2 at these interorganellar contact sites (58–60), it is established that deficiencies in MFN2 reduce MERCs (61–63). Consistent with this finding, we used an established proximity ligation assay (PLA) to confirm reductions in the number and size of MERCs in MFN2-deficient cells (Fig. 6*A* and *SI Appendix*, Fig. S6*A*) (10). Treatment with the ISR activators HF or PGL increased the size, but not the number, of MERCs in wild-type U2OS cells (*SI Appendix*, Fig. S6 *B–D*). However, treatment with these compounds restored both the size and number of MERCs in *MFN2*-deficient U2OS cells to levels similar or greater than those observed in wild-type cells (Fig. 6 *B–D*). Cotreatment with ISRIB blocked these increases. Similar effects were observed in wild-type and *Mfn2*-deficient MEFs treated with these ISR activators (*SI Appendix*, Fig. S6 *E–J*). These results show that pharmacologic ISR activation rescues MERCs in MFN2-deficient cells.

Apart from the CMT2A-associated phenotypes described above, deficiencies in MFN2 also reduces the basal oxygen consumption rate (OCR) in MEF and U2OS cells, as measured using the Resipher system (Fig. 6 *E* and *F*). Thus, we sought to define the potential for pharmacologic ISR activation to restore respiratory activity in these cells. Treatment with HF or PGL increased OCR in wild-type cells through an ISRIB-sensitive mechanism (*SI Appendix*, Fig. S6 *K* and *L*). Similarly, we observed increased OCR in MFN2-deficient MEF and U2OS cells treated with these compounds (Fig. 6 *E* and *F*). This increase was blocked by cotreatment with ISRIB. This finding indicates that, apart from morphologic aspects of mitochondrial biology, pharmacologic activation of the ISR using HF or PGL also enhances mitochondrial respiratory activity in MFN2-deficient cells.

Discussion

Here, we employed a drug repurposing screen to identify MBX-2982 (MBX) and parogrelil (PGL) as compounds that selectively activate the ISR through the OMA1-DELE1-HRI signaling pathway. We show that these compounds promote adaptive mitochondrial elongation that protects against mitochondrial fragmentation induced by chemical (e.g., CCCP) or genetic (e.g., *Perk* deficiency) insults. Further, we show that pharmacologic ISR activation afforded by the GCN2 activator halofuginone (HF) or, especially, the HRI activator PGL ameliorates mitochondrial dysfunctions including fragmentation, reduced motility, decreased ER–mitochondrial contacts, and impaired respiration in MFN2-deficient U2OS and MEF cells. These results establish MBX and PGL as highly selective ISR activating compounds and demonstrate the potential for pharmacologic ISR activation for correcting pathologic mitochondrial dysfunction in diseases associated with MFN2 deficiency such as CMT2A.

MBX and PGL are both previously identified drugs that successfully passed phase I clinical trials. MBX was originally described as a GPR119 agonist that was designed for the treatment of Type 2 diabetes (64), while PGL was identified as a PDE3 inhibitor that was developed for intermittent claudication (65, 66). Herein, we show that these compounds are highly selective activators of the ISR. However, it is unlikely that either compound activates ISR signaling through these previously reported activities. GPR119 is not expressed in the cell lines used in this study, indicating that MBX-dependent ISR activation is independent of its role in targeting this G-protein-coupled receptor. Further, the IC_{50} for PGL-dependent inhibition of PDE3 (0.26 nM) (66) is significantly lower than that observed for ISR activation (6.2 μM) and treatment with the alternative PDE3 inhibitor cilostazol (EC_{50} for PDE3 inhibition = 0.2 μM) does not induce expression of ISR target genes (e.g., *ASNS, CHAC1*) in HEK293T cells (*SI Appendix*, Fig. S6*M*). This discrepancy suggests that PGL does not activate the ISR through PDE3 inhibition. While efforts to identify the specific protein targets of these compounds required for ISR activation are currently ongoing,

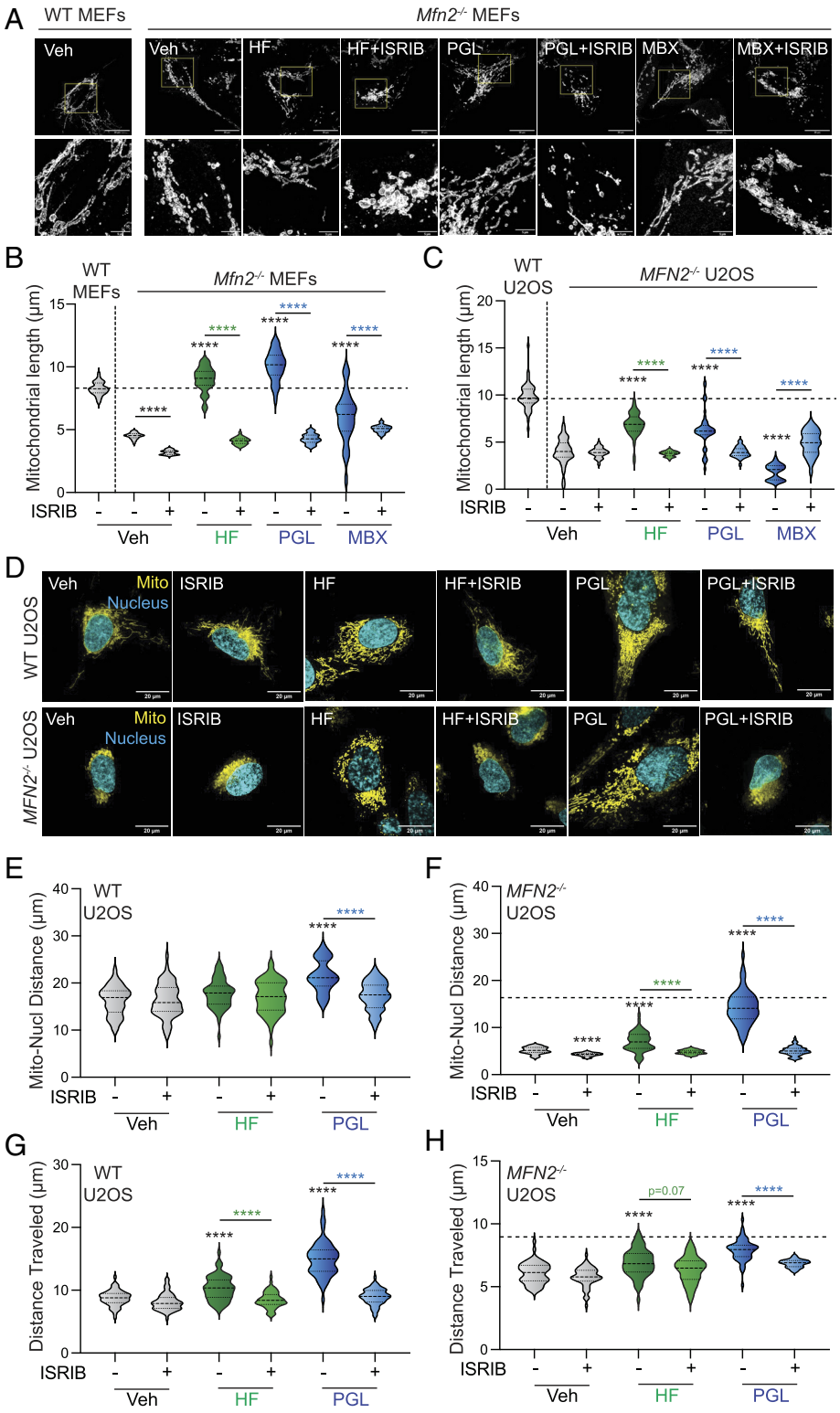

Fig. 5. Pharmacologic ISR activation rescues mitochondrial morphology and motility in *MFN2*-deficient cells. (*A* and *B*) Representative images (*A*) and quantification (*B*) of mitochondrial length in *Mfn2*-deficient MEFs treated for 6 h with halofuginone (HF; 100 nM); parogrelil (PGL; 10 μM), MBX-2982 (MBX; 10 μM), and/or ISRIB (200 nM) stained with TOMM20 antibodies. Vehicle-treated wild-type (WT) MEF cells are shown as a control. Violin plots show data from 60 images of cells collected across two independent experiments. (*C*) Quantification of mitochondrial length in fixed *MFN2*-deficient U2OS cells treated for 6 h with halofuginone (HF; 100 nM); parogrelil (PGL; 10 μM), MBX-2982 (MBX; 10 μM), and/or ISRIB (200 nM) stained with TOMM20 antibodies. Vehicle-treated wild-type (WT) U2OS cells are shown as a control. Representative images are shown in *SI Appendix*, Fig. S5*A*. Violin plots show data from 60 images of cells collected across two independent experiments. (*D*–*F*) Representative images (*D*) and quantification (*E* and *F*) of mitochondria-nuclear distance in wild-type U2OS cells or *MFN2*-deleted U2OS cells treated for 6 h with halofuginone (HF; 100 nM), parogrelil (PGL; 10 μM), and/or ISRIB (200 nM) stained with TOMM20 antibodies (yellow) and Hoechst (blue). The dashed line in (*F*) shows mitochondria-nuclear distance in vehicle-treated wild-type cells for comparison. Violin plots show data from 60 images of cells collected across two independent experiments. (*G* and *H*) Mitochondrial distance traveled, measured by time lapse live cell imaging, in wild-type (*Left*) or *MFN2*-deficient U2OS cells (*Right*) treated for 6 h with halofuginone (HF; 100 nM), parogrelil (PGL; 10 μM), and/or ISRIB (200 nM). The dashed line in (*H*) shows the distance traveled in vehicle-treated wild-type cells. Data shown were collected across two biological replicates. Violin plots show median and interquartile range. ****$P < 0.001$ for Brown–Forsythe and Welch ANOVA. Black asterisks indicate comparison to vehicle-treated cells. Colored asterisks indicate comparison to cells cotreated with ISRIB.

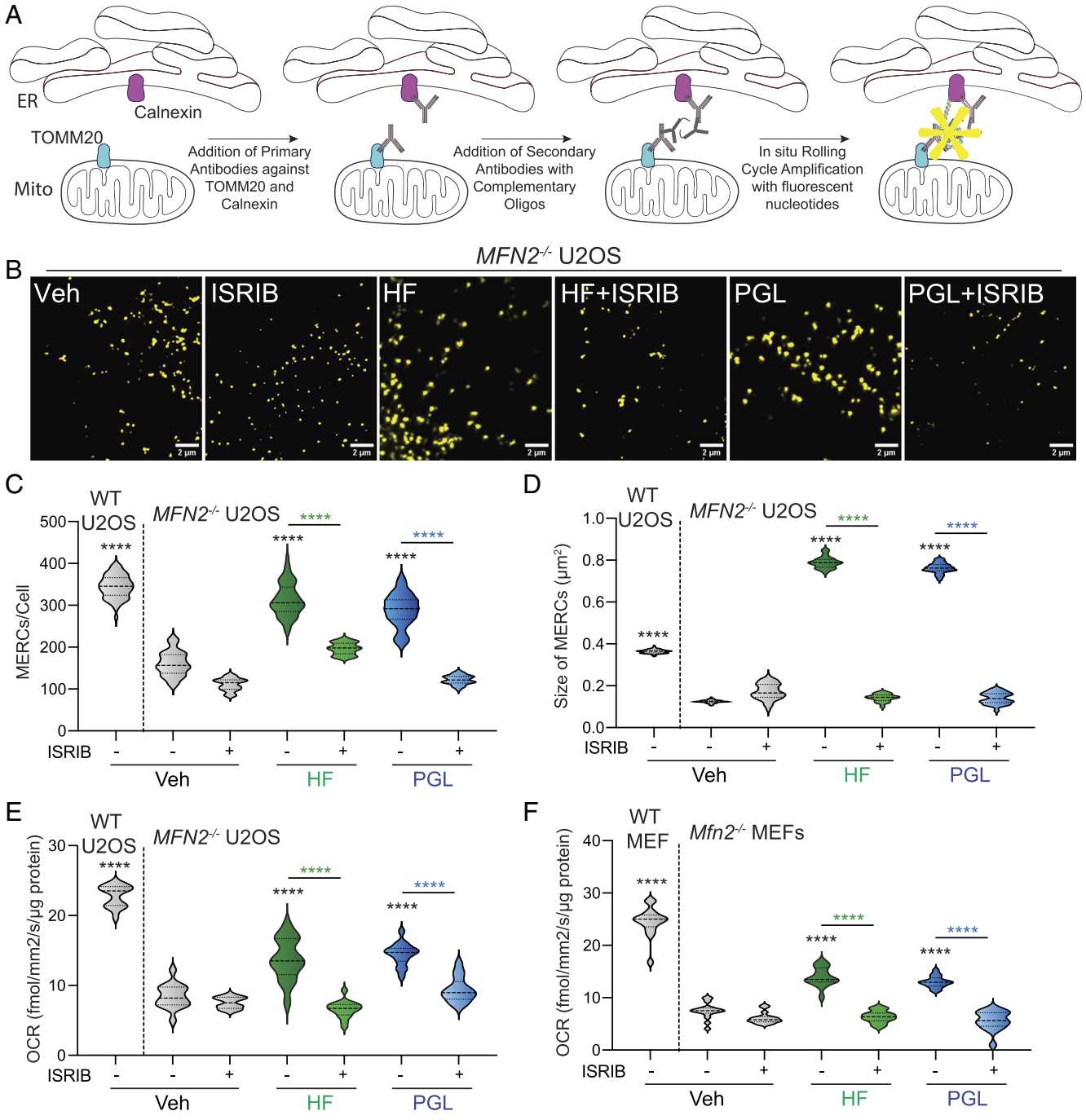

Fig. 6. ISR activating compounds restore ER–mitochondrial contacts and enhance respiration in MFN2-deficient cells. (*A*) PLA used to monitor ER–mitochondrial contact sites. (*B–D*) Representative images (*B*) and quantification of MERC number (*C*) and size (*D*), measured by PLA, in *MFN2*-deficient U2OS cells treated for 6 h with halofuginone (100 nM), parogrelil (PGL; 10 µM), and/or ISRIB (200 nM). PLA signal in wild-type U2OS cells is shown for comparison. Violin plots show data from 60 images of cells collected across two independent experiments. (*E* and *F*) Oxygen consumption rate (OCR), measured using the Resipher system, in MFN2-deficient U2OS (*E*) and MEF (*F*) cells treated for 6 h with halofuginone (HF; 100 nM), parogrelil (PGL, 10 µM), and/or ISRIB (200 nM). OCR in wild-type cells is shown as a control. Violin plots show data from 16 wells across two independent experiments. ****$P < 0.005$ for one-way ANOVA. Black asterisks show comparison with vehicle-treated cells and colored asterisks represent comparison with ISRIB cotreatment.

we show that both these compounds initiate ISR signaling through the mitochondrial stress-sensing OMA1-DELE1-HRI signaling axis. This finding is intriguing, as this signaling pathway has primarily been reported to be activated by mitochondrial stressors such as the uncoupler CCCP and the ATP synthase inhibitor oligomycin—treatments that also induce mitochondrial dysfunctions including organelle fragmentation, uncoupling, and impaired respiratory chain activity. In contrast, we show that activation of OMA1-DELE1-HRI signaling induced by MBX and PGL promotes adaptive ISR-dependent remodeling of mitochondria independent of these mitochondrial dysfunctions. This work highlights the potential for therapeutically accessing this endogenous mitochondrial stress-sensing mechanism to promote mitochondrial remodeling and mitigate mitochondrial dysfunction in different diseases.

While ISR-dependent translational and transcriptional signaling induced downstream of the four different ISR kinases is generally considered to be similar, recent work has begun to suggest that HRI activation may have unique functions involved in adapting

mitochondria during mitochondrial stress. Notably, HRI activation induced by iron chelation, but not stress-induced activation of other ISR kinases, was shown to promote PINK/PARKIN-independent mitophagy through a mechanism involving increased localization of phosphorylated eIF2α to the mitochondrial outer membrane (67). While our results show that pharmacologic activation of GCN2 with HF or HRI with PGL show similar improvements in mitochondria biology across most assays, we did note that PGL preferentially improved mitochondrial motility in MFN2-deficient U2OS and MEF cells, as compared to HF. This observation suggests a previously unanticipated advantage for pharmacologically activating the ISR through the OMA1-DELE1-HRI pathway, using compounds like PGL, for mitigating mitochondrial dysfunctions such as reduced motility associated with CMT2A and related diseases.

Intriguingly, despite activating the ISR through OMA1-DELE1-HRI signaling and promoting adaptive mitochondrial elongation in wild-type cells, MBX demonstrated a synthetic interaction with MFN2 deficiency that limited its application for improving outcomes in cells lacking MFN2. This observation likely reflects an off-target activity of MBX, such as the MBX-dependent increase in cholesterol biosynthesis genes observed in our RNAseq analysis. Previous work has highlighted a role for MFN2 in regulating cholesterol, potentially explaining the synthetic interaction between MBX and MFN2 deficiency observed in our study (68–71). While MBX did not prove beneficial for correcting mitochondrial morphology in MFN2-deficient cells, this compound did ameliorate mitochondrial fragmentation induced by mitochondrial uncoupling or *Perk* deficiency. This finding, combined with the selectivity of MBX for ISR activation, suggests that this compound could be useful for probing the potential of pharmacologic ISR activation to ameliorate mitochondrial dysfunction induced by other types of pathologic insults.

No therapeutic approaches are currently available to mitigate pathologic mitochondrial dysfunction associated with MFN2 deficiency in CMT2A. In MFN2-deficient cells, PGL and HF improved three MFN2-associated functions implicated in CMT2A pathology: mitochondrial fragmentation, mitochondrial motility, and ER–mitochondrial contacts. Further, PGL and HF enhanced respiratory chain activity in MFN2-deficient cells. This finding suggests that treatment with these compounds could similarly ameliorate the myriad mitochondrial dysfunctions induced by both mutations that completely ablate MFN2 activity and hypomorphic CMT2A-associated MFN2 mutants that retain partial function (8). While most CMT2A MFN2 variants do not have deficient mitochondrial respiration, the fact that mitochondrial respiration was rescued in MFN2 deficient cells augurs well for the promise of ISR activation to rescue MFN2 dysfunction in CMT2A. Consistent with this notion, previous work has shown that HF-dependent ISR activation restores mitochondrial tubular morphology in patient fibroblasts expressing hypomorphic $MFN2^{D414V}$ (34). As we continue the development of this approach, it will be exciting to further probe the scope of CMT2A-associated MFN2 mutants that can be rescued by pharmacologic ISR activation using PGL and HF in patient-derived and animal models of disease.

A challenge in translating pharmacologic ISR activators for diseases such as CMT2A is the potential for chronic activation of this pathway to lead to pathologic ISR signaling. However, pharmacologic ISR activation using compounds such as HF is well tolerated in vivo, highlighting the potential for the continued development of this approach (72–74). Further, both MBX and PGL have passed phase I clinical trials with good safety records, reflecting the in vivo potential for pharmacologic ISR activation using these compounds (66, 75). As we continue developing pharmacologic ISR activators for CMT2A, and related diseases involving mitochondrial dysfunction, we will optimize pharmacokinetic and pharmacodynamic profiles of ISR activators to allow for the selective activation of adaptive, protective ISR signaling independent of chronic, pathologic ISR signaling, as we have for other stress pathway activators (76, 77). Thus, as we advance the development of these classes of compounds through medicinal chemistry efforts focused on optimizing potency and selectivity for ISR activation, we will be able to further establish pharmacologic ISR activation as a viable strategy to mitigate mitochondrial dysfunction associated with etiologically diverse diseases.

Materials and Methods

ReFRAME Screen. To complete the primary screen of the ReFRAME library, the ATF4-FLuc ISR reporter stably expressed in HEK293T cells were plated into 1,536 well, with solid bottom Geiner plates with 750 cells per well in 5 μL of media. After allowing the cells to adhere overnight, the ReFRAME library compounds were transferred to the plates using Echo acoustic transfer to deliver 5 nL of compound per well, with a final screening concentration of 10 μM. After 24 h, 5 μL of OneGlo (Promega) was added, the plates were centrifuged, incubated 10 min, and quantified using the Luminescence module on the Pherastar (BMG). All hits which met the cut off criteria were picked for hit confirmation in 10 point dose–response curves, with a 1:3 dilution, beginning at 10 μM as the top dose in triplicate. All confirmed hits which had an $EC_{50} < 10$ μM were evaluated in subsequent experiments.

Fluorescence Microscopy. MEF^{mtGFP} and $Perk^{+/+}$ and $Perk^{-/-}$ MEFs were seeded at a density of 15,000 cells per well in eight-chamber slides (Ibidi) coated with poly-d-lysine (Sigma). The next day cells were treated with the indicated dose of compound for the indicated time. After treatment, cells were imaged on a Zeiss LSM 880 Confocal Laser Scanning Microscope equipped with a full incubation chamber for regulating temperature and CO_2 during live-cell imaging. $Perk^{+/+}$ and $Perk^{-/-}$ MEFs were visualized by staining with TMRE (Thermofisher). Mitochondrial bounding box length and sphericity were quantified using the Imaris software, as previously described (34).

Mitochondrial network morphology in wild-type and *Mfn2* KO MEFs and wild-type and *MFN2*-deficient U2OS cells was analyzed using immunofluorescence labeling. 20,000 cells were seeded in 12 mm coverslips and grown for 24 h. Following compound treatment for 6 h, cells were subsequently fixed with 4% paraformaldehyde, permeabilized with 0.1% Triton X-100 and blocked with 10% fetal bovine serum (FBS). The mitochondrial network was labeled using rabbit anti-TOMM20 (Abcam; ab186735) and visualized using anti-rabbit Alexa Fluor 488 (Thermo Fisher Scientific; A-11029). Coverslips were mounted using ProLong Diamond Anti-Fade mounting media (Invitrogen; P36965). Imaging was done using an Olympus Spinning Disk Confocal System (Olympus SD-IX83-SPINSR) using a 60× oil immersion objective. A cellVivo live cell incubator system was used for live cell imaging at 37 °C and 5% CO_2. Mitochondrial branch length was analyzed using the MiNA plugin (78) on FIJI (79) Particle number and size were calculated using the Analyze Particles plugin on FIJI while Mito-nucleus distances were calculated as previously described for nucleus-lipid droplet distances (9).

PLA. Mito–ER contact sites were visualized using a previously established PLA (10). Briefly, MEF and U2OS cells were seeded at a density of 30,000 cells per well in coverslips and grown for 24 h. Following treatment with compounds for the indicated time, cells were fixed with PFA, permeabilized, and blocked using the Duolink Blocking buffer from the PLA kit (DUI92008; Sigma-Aldrich). This step was followed by incubation with the primary antibodies (anti-TOMM20 for mitochondria and anti-Calnexin for the ER) overnight and subsequently with anti-mouse (DUO92004; Sigma-Aldrich) and anti-rabbit (DUO92002; Sigma-Aldrich) PLA probes. Manufacturer's instructions were followed for addition of ligase and polymerase from the PLA kit. Secondary antibodies were added to visualize the mitochondria (AlexaFluor 488, A-11029; Thermo Fisher Scientific) and ER (AlexaFluor 647, A-21245; Thermo Fisher Scientific). The coverslips were mounted with ProLong Diamond Antifade Mountant before imaging.

OCR. OCRs were measured using the Lucid Resipher system. Wild-type and MFN2-deficient MEF and U2OS cells were seeded at a density of 15,000 cells per well in a 96-well plate and allowed to settle for 24 h. Subsequently, drugs

were added at the indicated concentrations and the lid was attached to the plate, which was attached to the hub. The OCR was measured at 6 h and normalized to total protein present in the well. Total protein was calculated by collecting cells from each well, lysed using radioimmunoprecipitation assay (RIPA) buffer (89901; Fisher Scientific) and quantified using the bicinchoninic acid (BCA) assay, normalized to bovine serum albumin (BSA).

Additional Materials and Methods are included in the *SI Appendix*.

Data, Materials, and Software Availability. RNAseq data have been deposited in European Nucleotide Archive (ENA) repository (PRJEB101602) (80). All study data are included in the article and/or supporting information.

ACKNOWLEDGMENTS. We thank Xiaoyan Guo for providing the *OMA1* and *DELE1* knockout HEK293T cell lines used in this study and Martin Kampmann for providing the HEK293T cells expressing ATF4-mAPPLE with individual ISR kinases CRISPRi-depleted. We thank Ilia Droujinine for comments on the manuscript, and the microscopy and genomic cores at TSRI for experimental support. We also thank the Wellcome Trust and the Bill & Melinda Gates Foundation for their support of the ReFRAME library. This work was supported by the NIH (NS095892, NS125674, and AG088908 to R.L.W.), the Canadian Institutes of Health Research (to T.E.S.), George E. Hewitt Foundation Postdoctoral Fellowship (to P.B.), a Hotchkiss Brain Institute International Graduate Recruitment Scholarship (to M.Z.), a NSF Predoctoral Fellowship (to S.O.), and an American Heart Association Predoctoral Fellowship (to P.M.).

Author affiliations: [a]Department of Molecular and Cellular Biology, The Scripps Research Institute, La Jolla, CA 92037; [b]Department of Biochemistry and Molecular Biology, Cummings School of Medicine, University of Calgary, Calgary, AB T2N 4N1, Canada; [c]Department of Integrative Structural and Computational Biology, The Scripps Research Institute, La Jolla, CA 92037; [d]Calibr-Skaggs Institute for Innovative Medicines, The Scripps Research Institute, La Jolla, CA 92037; [e]Department of Medical Genetics, Cumming School of Medicine, Hotchkiss Brain Institute, Snyder Institute for Chronic Diseases, Alberta Children's Hospital Research Institute, University of Calgary, Calgary, AB T2N 4N1, Canada; and [f]Department of Biochemistry and Molecular Biology, Cumming School of Medicine, Hotchkiss Brain Institute, Snyder Institute for Chronic Diseases, Alberta Children's Hospital Research Institute, University of Calgary, Calgary, AB T2N 4N1, Canada

1. O. M. de Brito, L. Scorrano, Mitofusin 2 tethers endoplasmic reticulum to mitochondria. *Nature* **456**, 605–610 (2008).
2. A. Misko, S. Jiang, I. Wegorzewska, J. Milbrandt, R. H. Baloh, Mitofusin 2 is necessary for transport of axonal mitochondria and interacts with the Miro/Milton complex. *J. Neurosci.* **30**, 4232–4240 (2010).
3. C. R. Schiavon, G. S. Shadel, U. Manor, Impaired mitochondrial mobility in Charcot-Marie-Tooth disease. *Front. Cell Dev. Biol.* **9**, 624823 (2021).
4. H. Chen *et al.*, Mitofusins Mfn1 and Mfn2 coordinately regulate mitochondrial fusion and are essential for embryonic development. *J. Cell Biol.* **160**, 189–200 (2003).
5. M. Zaman *et al.*, A novel variant in MFN2 linked to a lethal disorder of neonatal onset. medRxiv [Preprint] (2024).
6. D. Loiseau *et al.*, Mitochondrial coupling defect in Charcot-Marie-Tooth type 2A disease. *Ann. Neurol.* **61**, 315–323 (2007).
7. S. Vielhaber *et al.*, Mitofusin 2 mutations affect mitochondrial function by mitochondrial DNA depletion. *Acta Neuropathol.* **125**, 245–256 (2013).
8. M. Zaman, T. E. Shutt, The role of impaired mitochondrial dynamics in MFN2-mediated pathology. *Front. Cell Dev. Biol.* **10**, 858286 (2022).
9. G. Sharma *et al.*, Characterization of a novel variant in the HR1 domain of MFN2 in a patient with ataxia, optic atrophy and sensorineural hearing loss. *F1000Res* **10**, 606 (2021).
10. M. Zaman *et al.*, The MFN2 Q367H variant reveals a novel pathomechanism connected to mtDNA-mediated inflammation. *Life Sci. Alliance* **8**, e202402921 (2025).
11. S. Zuchner *et al.*, Mutations in the mitochondrial GTPase mitofusin 2 cause Charcot-Marie-Tooth neuropathy type 2A. *Nat. Genet.* **36**, 449–451 (2004).
12. A. S. Carr *et al.*, MFN2 deletion of exons 7 and 8: Founder mutation in the UK population. *J. Peripher. Nerv. Syst.* **20**, 67–71 (2015).
13. G. A. Nicholson *et al.*, Severe early-onset axonal neuropathy with homozygous and compound heterozygous MFN2 mutations. *Neurology* **70**, 1678–1681 (2008).
14. J. M. Polke *et al.*, Recessive axonal Charcot-Marie-Tooth disease due to compound heterozygous mitofusin 2 mutations. *Neurology* **77**, 168–173 (2011).
15. G. Piscosquito *et al.*, Mutational mechanisms in MFN2-related neuropathy: Compound heterozygosity for recessive and semidominant mutations. *J. Peripher. Nerv. Syst.* **20**, 380–386 (2015).
16. S. L. Sawyer *et al.*, Homozygous mutations in *MFN2* cause multiple symmetric lipomatosis associated with neuropathy. *Hum. Mol. Genet.* **24**, 5109–5114 (2015).
17. S. A. Detmer, D. C. Chan, Complementation between mouse Mfn1 and Mfn2 protects mitochondrial fusion defects caused by CMT2A disease mutations. *J. Cell Biol.* **176**, 405–414 (2007).
18. C. Barsa, J. Perrin, C. David, A. Mourier, M. Rojo, A cellular assay to determine the fusion capacity of MFN2 variants linked to Charcot-Marie-Tooth disease of type 2 A. *Sci. Rep.* **15**, 9971 (2025).
19. N. Bernard-Marissal *et al.*, Altered interplay between endoplasmic reticulum and mitochondria in Charcot-Marie-Tooth type 2A neuropathy. *Proc. Natl. Acad. Sci. U.S.A.* **116**, 2328–2337 (2019).
20. R. H. Baloh, R. E. Schmidt, A. Pestronk, J. Milbrandt, Altered axonal mitochondrial transport in the pathogenesis of Charcot-Marie-Tooth disease from mitofusin 2 mutations. *J. Neurosci.* **27**, 422–430 (2007).
21. A. S. Saporta *et al.*, Charcot-marie-tooth disease subtypes and genetic testing strategies. *Ann. Neurol.* **69**, 22–33 (2011).
22. S. M. Murphy *et al.*, Charcot-Marie-Tooth disease: Frequency of genetic subtypes and guidelines for genetic testing. *J. Neurol. Neurosurg. Psychiatry* **83**, 706–710 (2012).
23. V. Fridman *et al.*, CMT subtypes and disease burden in patients enrolled in the Inherited Neuropathies Consortium natural history study: A cross-sectional analysis. *J. Neurol. Neurosurg. Psychiatry* **86**, 873–878 (2015).
24. Y. Zhou *et al.*, Restoring mitofusin balance prevents axonal degeneration in a Charcot-Marie-Tooth type 2A model. *J. Clin. Invest.* **129**, 1756–1771 (2019).
25. S. Shahin *et al.*, MFN1 augmentation prevents retinal degeneration in a Charcot-Marie-Tooth type 2A mouse model. *iScience* **26**, 106270 (2023).
26. F. Rizzo *et al.*, Combined RNA interference and gene replacement therapy targeting *MFN2* as proof of principle for the treatment of Charcot-Marie-Tooth type 2A. *Cell. Mol. Life Sci.* **80**, 373 (2023).
27. A. G. Rocha *et al.*, MFN2 agonists reverse mitochondrial defects in preclinical models of Charcot-Marie-Tooth disease type 2A. *Science* **360**, 336–341 (2018).
28. X. Dang *et al.*, Discovery of 6-phenylhexanamide derivatives as potent stereoselective mitofusin activators for the treatment of mitochondrial diseases. *J. Med. Chem.* **63**, 7033–7051 (2020).
29. X. Dang *et al.*, Pharmacophore-based design of phenyl-[hydroxycyclohexyl] cycloalkyl-carboxamide mitofusin activators with improved neuronal activity. *J. Med. Chem.* **64**, 12506–12524 (2021).
30. A. Franco, X. Dang, L. Zhang, P. B. Molinoff, G. W. Dorn II, Mitochondrial dysfunction and pharmacodynamics of mitofusin activation in murine Charcot-Marie-Tooth disease type 2A. *J. Pharmacol. Exp. Ther.* **383**, 137–148 (2022).
31. J. Weigele, L. Zhang, A. Franco, E. Cartier, G. W. Dorn II, Sensory-motor neuropathy in Mfn2 T105M knock-in mice and its reversal by a novel piperine-derived mitofusin activator. *J. Pharmacol. Exp. Ther.* **391**, 361–374 (2024).
32. M. Costa-Mattioli, P. Walter, The integrated stress response: From mechanism to disease. *Science* **368**, eaat5314 (2020).
33. K. Pakos-Zebrucka *et al.*, The integrated stress response. *EMBO Rep.* **17**, 1374–1395 (2016).
34. K. R. Baron *et al.*, Pharmacologic activation of integrated stress response kinases inhibits pathologic mitochondrial fragmentation. *Elife* **13**, RP100541 (2025).
35. J. Lebeau *et al.*, The PERK arm of the unfolded protein response regulates mitochondrial morphology during acute endoplasmic reticulum stress. *Cell Rep.* **22**, 2827–2836 (2018).
36. V. Perea *et al.*, Pharmacologic activation of a compensatory integrated stress response kinase promotes mitochondrial remodeling in PERK-deficient cells. *Cell Chem. Biol.* (2023), 10.1016/j.chembiol.2023.10.006.
37. V. Perea *et al.*, PERK signaling promotes mitochondrial elongation by remodeling membrane phosphatidic acid. *EMBO J.* **42**, e113908 (2023).
38. B. A. Barad, M. Medina, D. Fuentes, R. L. Wiseman, D. A. Grotjahn, A surface morphometrics toolkit to quantify organellar membrane ultrastructure using cryo-electron tomography. bioRxiv [Preprint] (2022).
39. P. Latorre-Muro *et al.*, A cold-stress-inducible PERK/OGT axis controls TOM70-assisted mitochondrial protein import and cristae formation. *Cell Metab.* **33**, 598–614.e7 (2021).
40. E. Balsa *et al.*, ER and nutrient stress promote assembly of respiratory chain supercomplexes through the PERK-eIF2alpha axis. *Mol. Cell* **74**, 877–890.e6 (2019).
41. E. Bobrovnikova-Marjon *et al.*, PERK utilizes intrinsic lipid kinase activity to generate phosphatidic acid, mediate Akt activation, and promote adipocyte differentiation. *Mol. Cell. Biol.* **32**, 2268–2278 (2012).
42. T. L. Keller *et al.*, Halofuginone and other febrifugine derivatives inhibit prolyl-tRNA synthetase. *Nat. Chem. Biol.* **8**, 311–317 (2012).
43. K. R. Carlson, M. M. Georgiadis, F. Tameire, K. A. Staschke, R. C. Wek, Activation of Gcn2 by small molecules designed to be inhibitors. *J. Biol. Chem.* **299**, 104595 (2023).
44. M. Szaruga *et al.*, Activation of the integrated stress response by inhibitors of its kinases. *Nat. Commun.* **14**, 5535 (2023).
45. A. P. Pitera, M. Szaruga, S. Y. Peak-Chew, S. W. Wingett, A. Bertolotti, Cellular responses to halofuginone reveal a vulnerability of the GCN2 branch of the integrated stress response. *EMBO J.* **41**, e109985 (2022).
46. J. Janes *et al.*, The reframe library as a comprehensive drug repurposing library and its application to the treatment of cryptosporidiosis. *Proc. Natl. Acad. Sci. U.S.A.* **115**, 10750–10755 (2018).
47. J. Yang *et al.*, DELE1 oligomerization promotes integrated stress response activation. *Nat. Struct. Mol. Biol.* **30**, 1295–1302 (2023).
48. C. Sidrauski *et al.*, Pharmacological brake-release of mRNA translation enhances cognitive memory. *Elife* **2**, e00498 (2013).
49. C. Sidrauski *et al.*, Pharmacological dimerization and activation of the exchange factor eIF2B antagonizes the integrated stress response. *Elife* **4**, e07314 (2015).
50. J. C. Tsai *et al.*, Structure of the nucleotide exchange factor eIF2B reveals mechanism of memory-enhancing molecule. *Science* **359**, eaaq0939 (2018).
51. A. F. Zyryanova *et al.*, Binding of ISRIB reveals a regulatory site in the nucleotide exchange factor eIF2B. *Science* **359**, 1533–1536 (2018).
52. J. M. D. Grandjean *et al.*, Deconvoluting stress-responsive proteostasis signaling pathways for pharmacologic activation using targeted RNA sequencing. *ACS Chem. Biol.* **14**, 784–795 (2019).
53. X. Guo *et al.*, Mitochondrial stress is relayed to the cytosol by an OMA1-DELE1-HRI pathway. *Nature* **579**, 427–432 (2020).
54. V. Perea *et al.*, Pharmacologic activation of a compensatory integrated stress response kinase promotes mitochondrial remodeling in PERK-deficient cells. Cell. *Chem. Biol.* **30**, 1571–1584 e1575 (2023).
55. J. J. Chen, HRI protein kinase in cytoplasmic heme sensing and mitochondrial stress response: Relevance to hematological and mitochondrial diseases. *J. Biol. Chem.* **301**, 108494 (2025).
56. E. Fessler *et al.*, A pathway coordinated by DELE1 relays mitochondrial stress to the cytosol. *Nature* **579**, 433–437 (2020).
57. H. P. Harding, Y. Zhang, A. Bertolotti, H. Zeng, D. Ron, Perk is essential for translational regulation and cell survival during the unfolded protein response. *Mol. Cell* **5**, 897–904 (2000).

58. D. Naon *et al.*, Critical reappraisal confirms that mitofusin 2 is an endoplasmic reticulum-mitochondria tether. *Proc. Natl. Acad. Sci. U.S.A.* **113**, 11249–11254 (2016).
59. R. Filadi *et al.*, On the role of mitofusin 2 in endoplasmic reticulum-mitochondria tethering. *Proc. Natl. Acad. Sci. U.S.A.* **114**, E2266–E2267 (2017).
60. D. Naon *et al.*, Reply to Filadi et al.: Does mitofusin 2 tether or separate endoplasmic reticulum and mitochondria? *Proc. Natl. Acad. Sci. U.S.A.* **114**, E2268–E2269 (2017).
61. V. Hertlein *et al.*, MERLIN: A novel BRET-based proximity biosensor for studying mitochondria-ER contact sites. *Life Sci. Alliance* **3**, e201900600 (2020).
62. S. Han *et al.*, The role of Mfn2 in the structure and function of endoplasmic reticulum-mitochondrial tethering in vivo. *J. Cell Sci.* **134**, jcs253443 (2021).
63. B. Gottschalk *et al.*, MFN2 mediates ER-mitochondrial coupling during ER stress through specialized stable contact sites. *Front. Cell Dev. Biol.* **10**, 918691 (2022).
64. R. M. Jones, J. N. Leonard, D. J. Buzard, J. Lehmann, GPR119 agonists for the treatment of type 2 diabetes. *Expert Opin. Ther. Pat.* **19**, 1339–1359 (2009).
65. M. Hori *et al.*, NT-702 (parogrelil hydrochloride, NM-702), a novel and potent phosphodiesterase 3 inhibitor, suppress the asthmatic response in guinea pigs, with both bronchodilating and anti-inflammatory effects. *Eur. J. Pharmacol.* **618**, 63–69 (2009).
66. N. Ishiwata *et al.*, NT-702 (parogrelil hydrochloride, NM-702), a novel and potent phosphodiesterase inhibitor, improves reduced walking distance and lowered hindlimb plantar surface temperature in a rat experimental intermittent claudication model. *Life Sci.* **81**, 970–978 (2007).
67. Y. Chakrabarty, Z. Yang, H. Chen, D. C. Chan, The HRI branch of the integrated stress response selectively triggers mitophagy. *Mol. Cell* **84**, 1090–1100.e6 (2024).
68. C. Liu *et al.*, Mitofusin 2 decreases intracellular lipids in macrophages by regulating peroxisome proliferator-activated receptor-gamma. *Biochem. Biophys. Res. Commun.* **450**, 500–506 (2014).
69. A. Bassot *et al.*, Loss and gain of function of Grp75 or mitofusin 2 distinctly alter cholesterol metabolism, but all promote triglyceride accumulation in hepatocytes. *Biochim. Biophys. Acta Mol. Cell Biol. Lipids* **1866**, 159030 (2021).
70. A. Kumar *et al.*, MFN2 coordinates mitochondria motility with alpha-tubulin acetylation and this regulation is disrupted in CMT2A. *iScience* **27**, 109994 (2024).
71. B. M. Garcia *et al.*, Glutamine sensing licenses cholesterol synthesis. *EMBO J.* **43**, 5837–5856 (2024).
72. S. Xu *et al.*, The clinical antiprotozoal drug halofuginone promotes weight loss by elevating GDF15 and FGF21. *Sci. Adv.* **11**, eadt3142 (2025).
73. S. Rai, M. Szaruga, A. P. Pitera, A. Bertolotti, Integrated stress response activator halofuginone protects mice from diabetes-like phenotypes. *J. Cell Biol.* **223**, e202405175 (2024).
74. M. J. de Jonge *et al.*, Phase I and pharmacokinetic study of halofuginone, an oral quinazolinone derivative in patients with advanced solid tumours. *Eur. J. Cancer* **42**, 1768–1774 (2006).
75. S. U. Kang, GPR119 agonists: A promising approach for T2DM treatment? A SWOT analysis of GPR119. *Drug Discov. Today* **18**, 1309–1315 (2013).
76. A. Madhavan *et al.*, Pharmacologic IRE1/XBP1s activation promotes systemic adaptive remodeling in obesity. *Nat. Commun.* **13**, 608 (2022).
77. E. A. Blackwood *et al.*, Pharmacologic ATF6 activation confers global protection in widespread disease models by reprograming cellular proteostasis. *Nat. Commun.* **10**, 187 (2019).
78. A. J. Valente, L. A. Maddalena, E. L. Robb, F. Moradi, J. A. Stuart, A simple ImageJ macro tool for analyzing mitochondrial network morphology in mammalian cell culture. *Acta Histochem.* **119**, 315–326 (2017).
79. J. Schindelin *et al.*, Fiji: An open-source platform for biological-image analysis. *Nat. Methods* **9**, 676–682 (2012).
80. L. Wiseman, The Scripps Research Institute, drug repurposing screen identifies an HRI activating compound that promotes adaptive mitochondrial remodeling in MFN2-deficient cells project. European Nucleotides Archive (ENA). https://www.ebi.ac.uk/ena/browser/view/PRJEB101602. Deposited 24 October 2025.